INTERNATIONAL JOURNAL FOR NUMERICAL METHODS IN FLUIDS
Int. J. Numer. Meth. Fluids 2007; **55**:589–610
Published online 20 March 2007 in Wiley InterScience (www.interscience.wiley.com). DOI: 10.1002/fld.1482

A comparative study of inflow conditions for two- and three-dimensional spatially developing mixing layers using large eddy simulation

W. A. McMullan*,†, S. Gao and C. M. Coats

Department of Engineering, University of Leicester, University Road, Leicester LE1 7RH, U.K.

SUMMARY

A series of spatially developing mixing layers are simulated using the large eddy simulation (LES) technique. A hyperbolic tangent function and data derived from boundary layer simulations are used to generate the inflow condition, and their effects on the flow are compared. The simulations are performed in both two and three dimensions. In two-dimensional simulations, both types of inflow conditions produce a layer that grows through successive pairings of Kelvin–Helmholtz (K–H) vortices, but the composition ratio is lower for the hyperbolic tangent inflow simulations. The two-dimensional simulations do not undergo a transition to turbulence. The three-dimensional simulations produce a transition to turbulence, and coherent structures are found in the post-transition region of the flow. The composition ratio of the three-dimensional layers is reduced in comparison to the counterpart two-dimensional runs. The mechanisms of growth are investigated in each type of simulation, and amalgamative pairing interactions are found in the pre-transition region of the three-dimensional simulations, and throughout the entire computational domain of those carried out in two-dimensions. The structures beyond the post-transition region of the three-dimensional simulations appear to behave in a much different manner to their pre-transition cousins, with no pairing-type interactions observed in the turbulent flow. In order to accurately simulate spatially developing mixing layers, it is postulated that the inflow conditions must closely correspond to the conditions present in the reference experiment. Copyright © 2007 John Wiley & Sons, Ltd.

Received 15 August 2006; Revised 27 November 2006; Accepted 11 February 2007

KEY WORDS: mixing layer; large eddy simulation; growth mechanisms; vortex structures; inflow condition

1. INTRODUCTION

The mixing layer that forms between merging fluid streams of differing velocity (and densities) is often regarded as the simplest form of free shear flow. Given this stature, it is somewhat surprising to note that there are still several questions that remain unanswered about its evolutionary

*Correspondence to: W. A. McMullan, Department of Engineering, University of Leicester, University Road, Leicester LE1 7RH, U.K.
†E-mail: wam3@le.ac.uk

nature—most notably the effects of inflow conditions upon the growth rate of the layer [1–4], and the effects of the presence of quasi-two-dimensional coherent structures found in the turbulent region of the flow [5–7].

The controlled environment that numerical simulations offer should provide some of the answers to the above issues. However, the overall topic of numerical research into mixing layer flows is somewhat confused by a number of problems. Firstly, there exist two distinct methods of simulating the mixing layer flow—temporally evolving and spatially developing simulations. In temporally evolving simulations, the flow develops in time within the computational domain, allowing the imposition of periodic boundary conditions in the stream- and spanwise directions, resulting in a very low computational cost [8]. This type of simulation technique has long been thought to produce flow patterns that provide quantitative comparisons with experiment. The formation of Kelvin–Helmholtz rollers [9], the development of the secondary streamwise instability [10, 11], and the interactions between the structures that eventually produce the transition to turbulence [12] have all been captured in temporal simulations. However, Taylor's hypothesis does not allow the transformation of time onto a spatial domain for such flows, as shown by Lebœuf and Metha [13]. They demonstrated that the spanwise and streamwise vorticity decay with streamwise distance, thus basing transforms on Taylor's hypothesis results in errors of $\sim$20–40%, far greater than previous estimates of $\sim$15%. The viability of temporal mixing layer simulations is also hindered by the symmetric entrainment of fluid from both sides of the layer, in contradiction to what is found experimentally [7]. In addition, the development of the temporally evolving layer is only influenced by the initial conditions and previous flow development—in the real mixing layer, the flow is influenced by events taking place downstream, in the form of low-frequency feedback. In order to capture these properties of the mixing layer, therefore, spatially developing simulations (in which the flow develops with downstream distance) must be conducted. Whilst spatially developing mixing layer simulations should offer a direct comparison with experimental work, the requirement of specifying a non-reflective boundary condition at the outflow plane of the domain greatly adds to the computational cost of the simulation. Past research into the numerical simulation of spatially developing mixing layers is very sparse, with most of the work focusing on validating numerical schemes [14–16]. To the authors' knowledge, only one study has focused on proving the large eddy simulation (LES) methodology for use in simulating fully three-dimensional mixing layers that undergo transition to turbulence [17].

Secondly, there is no particular consensus that defines the best inflow condition with which the mixing layer flow simulation should be initialized. Analytical hyperbolic tangent profiles [14, 18, 19], time-dependent inflow data from precursor boundary layer (BL) simulations [20], and analytical BL profiles [16, 21] have all been used to describe the initial condition of the flow in both direct numerical simulation (DNS) and LES, with each study giving reasonably good comparisons with their respective reference experiments. Mixing layer flows, however, are known to exhibit a hypersensitivity to their initial conditions [3, 22], and it is reasonable to assume that the simulated mixing layer will also display this behaviour. Balaras *et al.* [23] have shown that the evolution of temporal mixing layers is significantly affected by the nature of the inflow condition, whilst Tenaud *et al.* [16] demonstrated that the use of an analytical Whitfield profile [24] to describe a turbulent inflow condition required large freestream disturbance values to produce a growth rate in the layer that was comparable to experiment. For mixing layers that initiate from laminar conditions, there has been no direct comparison on the effects of using a hyperbolic tangent or boundary layer profile to describe the inflow condition of the layer. A series of simulations performed by Vreman *et al.* [19], demonstrated the viability of hyperbolic tangent inflow conditions for a low

DOI: 10.1002/fld

Reynolds number temporal mixing layer flow, initiated from laminar conditions, in comparison with a reference DNS. It should be noted, however, that only a hyperbolic tangent inflow profile was used in the reference DNS, whilst no effort was apparently made to quantify the effects of a BL-type inflow condition on the flow.

Thirdly, there is a common theme apparent in spatially developing simulations, with many researchers believing that two-dimensional simulations of the mixing layer flow yield results that are quantitatively comparable with experiment. Since the discovery of quasi-two-dimensional coherent structures in the turbulent flow, it has been thought that the growth of the mixing layer is dominated by two-dimensional processes, hence two-dimensional simulations should be able to capture the physics of the flow. Indeed, the mixing layer is often categorized as an example of the so-called two-dimensional turbulence [25]. Several publications conclude that such two-dimensional simulations accurately capture the dynamics of the flow in regions that are far downstream of where the transition to turbulence occurred in their reference experiments [14, 15, 21, 26–29]. All of the results presented in these publications show discrepancies with the real flow, implying that some differences may exist between the evolution of the flow in the simulation and in the experiment.

The present study focuses on assessing the performance of two of the inflow conditions described above—a hyperbolic tangent function, and time-dependent inflow data obtained from precursor BL simulations. Details of these inflow conditions will be given in Section 3. In addition, both two- and three-dimensional simulations of the mixing layer will be performed in order to quantify the effects of confining the flow to only two dimensions, and test the validity of claims that such simulations accurately represent the real flow. The simulations correspond to experiments performed by D'Ovidio [30], for several values of the velocity parameter λ, defined as

$$\lambda = \frac{U_1 - U_2}{U_1 + U_2} \tag{1}$$

where U_1 and U_2 are the freestream velocities on the high- and low-speed side of the layer, respectively.

2. NUMERICAL METHODS

The spatially filtered analytic equations for conservation of momentum and mass for a uniform density fluid are:

$$\frac{\partial \bar{u}_i}{\partial t} = -\frac{\partial \bar{p}}{\partial x_i} + \frac{\partial}{\partial x_j}(-\bar{u}_i \bar{u}_j + 2\nu \bar{S}_{ij}) \tag{2}$$

$$\bar{S}_{ij} = \frac{1}{2}\left(\frac{\partial \bar{u}_i}{\partial x_j} + \frac{\partial \bar{u}_j}{\partial x_i}\right) \tag{3}$$

$$\frac{\partial \bar{u}_i}{\partial x_i} = 0 \tag{4}$$

These equations are discretized on a staggered mesh as per Roache [31]. The viscosity ν can consists of both a molecular and a subgrid component, $\nu = \nu_m + \nu_{sg}$, if a subgrid-scale model is used. The governing equations are advanced in time using the Adams–Bashforth technique, accurate to

DOI: 10.1002/fld

second order

$$\bar{u}_i^* = \bar{u}_i^n + \Delta t(\tfrac{3}{2}H_i^n - \tfrac{1}{2}H_i^{n-1}) \tag{5}$$

with

$$H_i = \frac{\partial}{\partial x_j}(-\bar{u}_i\bar{u}_j + 2\nu\bar{S}_{ij}) \tag{6}$$

The provisional velocity $\bar{u}_i^*$ does not obey continuity and is updated to the actual velocity at the next time step, $\bar{u}_i^{n+1}$, by the pressure solver. The pressure field is solved implicitly by the use of the continuity equation. The provisional velocity field of $\bar{u}_i^*$ is used to derive the actual velocity by including the gradient of an unknown pressure field $\bar{p}^{n+1/2}$, such that

$$\bar{u}_i^{n+1} = \bar{u}_i^* - \Delta t\frac{\partial \bar{p}^{n+1/2}}{\partial x_i} \tag{7}$$

As the new velocity field must have zero divergence, a Poisson equation can be found for the pressure field between the present and next time step

$$\nabla^2 \bar{p}^{n+1/2} = \frac{1}{\Delta t}\frac{\partial \bar{u}_i^*}{\partial x_i} \equiv R \tag{8}$$

As the current code requires that one spatial dimension be periodic, a Fourier transform can be performed on Equation (8) to give a sequence of Helmholtz problems for each wave number k_z

$$\frac{\partial^2 \tilde{p}}{\partial x^2} + \frac{\partial^2 \tilde{p}}{\partial y^2} - k_z^2\tilde{p} = \tilde{R} \tag{9}$$

The Fourier transform is performed in one direction and is then iterated by a novel multigrid method for the other two directions to maximize the speed of convergence.

A passive scalar is also introduced into the flow domain, which is governed by the equation

$$\frac{\partial \bar{T}}{\partial t} = \frac{\partial}{\partial x_i}\left(-\bar{u}_i\bar{T} + \alpha\frac{\partial \bar{T}}{\partial x_i}\right) \tag{10}$$

where α is the diffusivity, which can contain both a molecular and a subgrid component, $\alpha = \alpha_m + \alpha_{sg}$, if a subgrid-scale model is used. With a subgrid-scale model employed, the subgrid diffusivity is set to $\alpha_{sg} = \nu_{sg}/0.3$. The scalar is discretized on the staggered mesh at the cell centre, and a second-order upwinding scheme is used to calculate the scalar flux between cell faces, following the work of Gao and Voke [32]—this is found to reduce overshoots in the scalar field to less than 5%. The Adams–Bashforth method is used to integrate the scalar field forward in time, with a method of discretization very similar to Equations (5)–(6).

3. FLOW SIMULATIONS

The simulations presented here are based on the experimental work of D'Ovidio [30]. Several mixing layer flows of differing λ were studied, and these are reproduced in the numerical simulations presented here. The simulations themselves are separated into two categories—two-dimensional and three-dimensional simulations. Within these two simulation types, there are two further sub-categories—simulations conducted with a hyperbolic tangent function specified as the inflow

DOI: 10.1002/fld

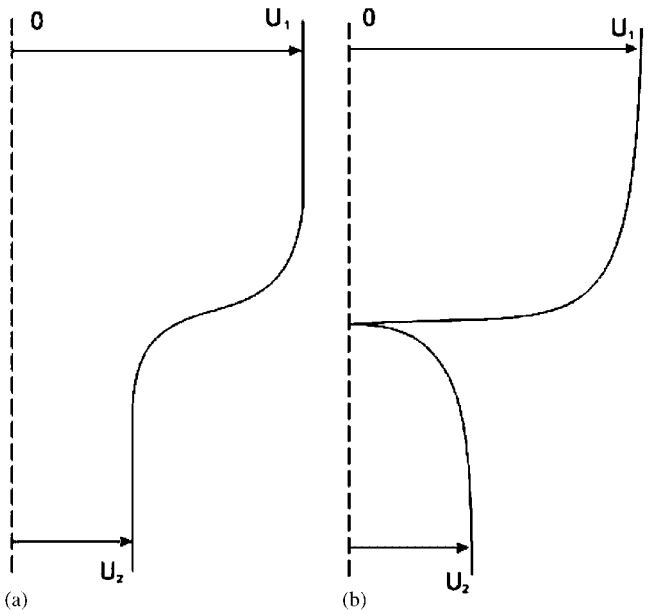

Figure 1. Schematic diagram of inflow profiles used for the present simulations: (a) hyperbolic tangent function and (b) boundary layer profiles.

condition, given by the equation

$$\bar{u}(y) = \frac{U_1 + U_2}{2} + \frac{U_1 - U_2}{2} \tanh\left(\frac{2y}{\delta_i}\right) \tag{11}$$

where δ_i is the initial vorticity thickness of the layer, and simulations where the inflow condition is derived from precursor two-dimensional BL simulations. The BL simulations are conducted on a computational grid of 0.3×0.038 m, with 128×64 cells used. The Smagorinsky subgrid-scale model, with $C_s = 0.1$ was used in these runs, in conjunction with a van Driest damping function to produce the correct near-wall eddy viscosity behaviour. In these BL runs, a *slicing plane* is chosen at the position where the momentum thickness of the boundary layer matches that reported in the experiment, and data are recorded at every time step at this plane. These slicing plane data are then interpolated onto the mixing layer mesh in a manner that strictly conserves mass flux. A schematic view of both types of inflow profile is shown in Figure 1. Due to the number of simulations conducted, they are named according to their defining properties, i.e. F58-BL-CS-3D is a simulation of Case F58, using BL inflow data, and simulated in three dimensions. Other simulations with the suffix HT denote simulations with a hyperbolic tangent inflow condition. The letters CS state that the subgrid-scale model used follows that of Smagorinsky [33], such that

$$\nu_{sg} = (C_s \bar{\Delta})^2 |\bar{S}| \tag{12}$$

where $|\bar{S}| = (2S_{ij}S_{ij})^{1/2}$, S_{ij} is the filtered strain-rate tensor, C_s is the Smagorinsky coefficient, and $\bar{\Delta}$ is the cut-off length. The evolution of the flow has been shown to be largely unaffected by the use of the Smagorinsky [33], Germano *et al.* [34], and Lilly [35], or structure function model [36] on the current mesh [37], hence the Smagorinsky model is used here for reasons of low computational cost. The parameter C_s is given a value of 0.12 in all simulations.

DOI: 10.1002/fld

Table I. Flow parameters of the mixing layers simulated.

Experiment number	U_1 (m s^{-1})	U_2 (m s^{-1})	λ	Δt (μs)
F9	31.39	12.96	0.42	1.2
F33	28.46	9.68	0.49	1.5
F58	19.93	6.81	0.49	1.6
HW9	32.12	9.59	0.54	1.2
FP42	21.58	5.19	0.61	1.6

In the three-dimensional simulations, the mesh used incorporates $256 \times 96 \times 64$ cells, with the domain size set to $0.16 \times 0.038 \times 0.03$ m. The mesh is stretched gently in the x- and y-directions in order to allow increased resolution in the plane of the splitter plate, although the splitter plate itself does not extend into the computational domain, as this would require the use of an internal wall boundary condition. The two-dimensional simulations use one cell in the spanwise domain, in order to force two-dimensionality onto the flow.

Several mixing layer flows are simulated, and their bulk properties are summarized in Table I, including the time step of each simulation. Each simulation is run for $120000\Delta t$, with the time steps varying between simulations. This is due to the requirement that the CFL number [38], given by

$$C = \Delta t \left(\frac{\bar{u}}{\Delta x} + \frac{\bar{v}}{\Delta y} + \frac{\bar{w}}{\Delta z} \right) \tag{13}$$

be kept below the stability limit. In all simulations, the maximum reported CFL number does not exceed 0.25. The two- and three-dimensional simulations of each case use the same time step, as approximately 60% of the CFL value comes from the cross-stream component $\bar{v}/\Delta y$. The passive scalar is injected into the flow at the inflow plane and is given a value of '0' on the low-speed side, and '1' on the high-speed side of the layer. In all simulations, the lateral boundaries are of an impermeable free-slip nature, and the spanwise boundaries are necessarily periodic. The outflow condition is of an advective form, given by the equation

$$\frac{\partial \bar{u}_x}{\partial t} = -U_c \frac{\partial \bar{u}_x}{\partial x} \tag{14}$$

where the derivative $\partial \bar{u}_x / \partial x$ is necessarily one-sided, and U_c is the mean streamwise velocity at the outflow plane. In order to conserve mass flux through the computational domain and retain the stability of the pressure solver, the mass flux at the outflow is compared with that of the inflow at each time step. If the two values are not equal the outflow velocity is normalized by the ratio of the inflow to outflow mass fluxes. The outflow boundary condition of the passive scalar is also treated in a very similar manner to that of the velocity field.

4. RESULTS

4.1. Two-dimensional simulations

The mean flow properties of the mixing layer are presented in a self-similar co-ordinate system, η, defined by

$$\eta = \frac{(y - y_{0.5})}{(x - x_0)} \tag{15}$$

DOI: 10.1002/fld

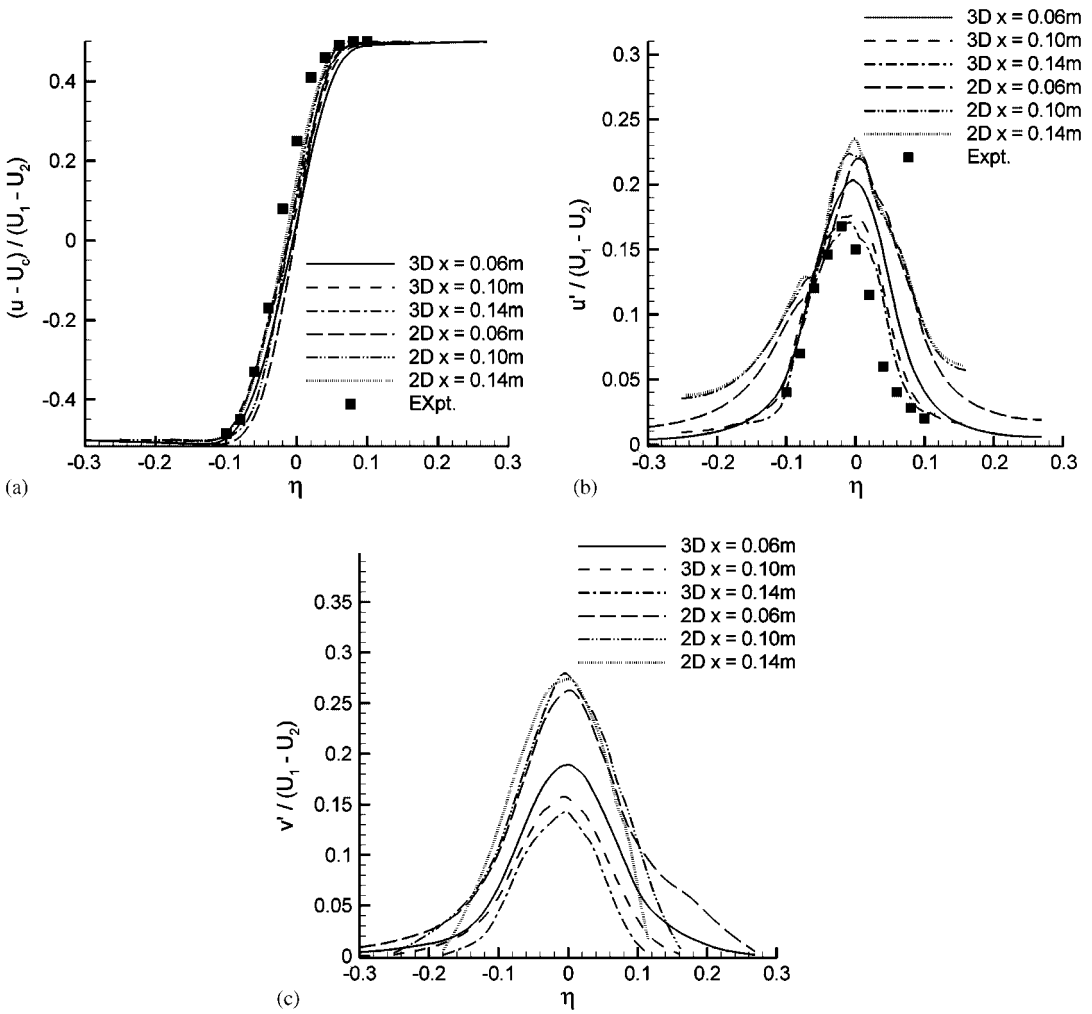

Figure 2. Mean and RMS fluctuation velocity profiles for cases HW9-BL-CS-2D and HW9-BL-CS-3D.

where $y_{0.5}$ is the lateral position where the streamwise velocity is equal to the mean of the freestream velocities, $U_a = (U_1 + U_2)/2$, and x_0 is the virtual origin of the mixing layer.

Typical mean and root mean squared (RMS) velocity and scalar field profiles for the two-dimensional simulations are shown in Figures 2 and 3, taken from case HW9-BL-CS-2D. Experimental profiles are also shown for the properties where these data are available. The mean streamwise velocity profiles agree well with the experiment, and the streamwise velocity fluctuations do not exhibit particularly good self-similar properties, as the profiles do not collapse onto a single line. This phenomenon is commonly found in two-dimensional mixing layer simulations [14, 39]. The mean scalar and RMS scalar fluctuation profiles bear a good resemblance to those produced by Zhou and Pereira [21], with the kink in the mean scalar profile, and the bimodal distribution of the fluctuation profile being characteristic of the two-dimensional, unsteady laminar flow.

DOI: 10.1002/fld

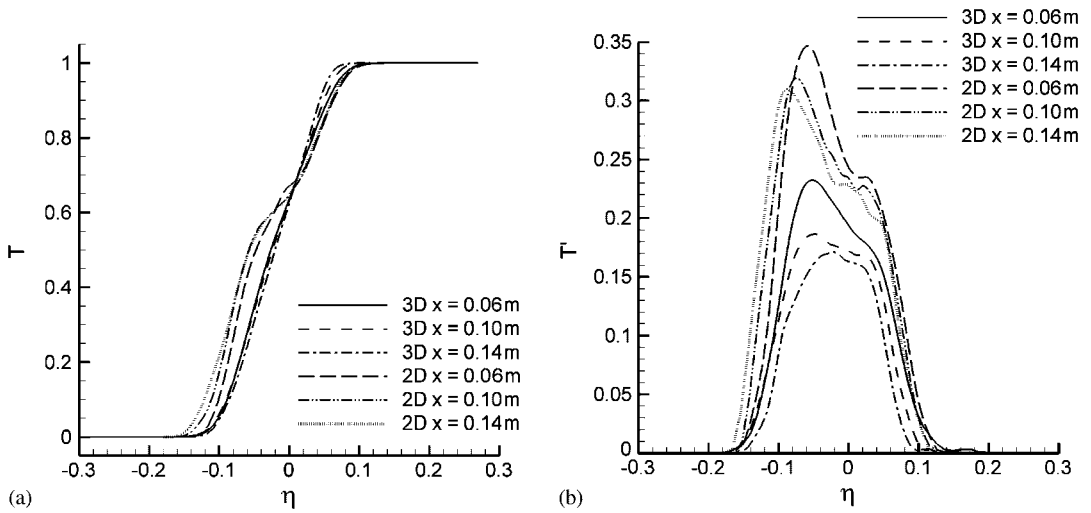

Figure 3. Mean and RMS fluctuation scalar profiles for cases HW9-BL-CS-2D and HW9-BL-CS-3D.

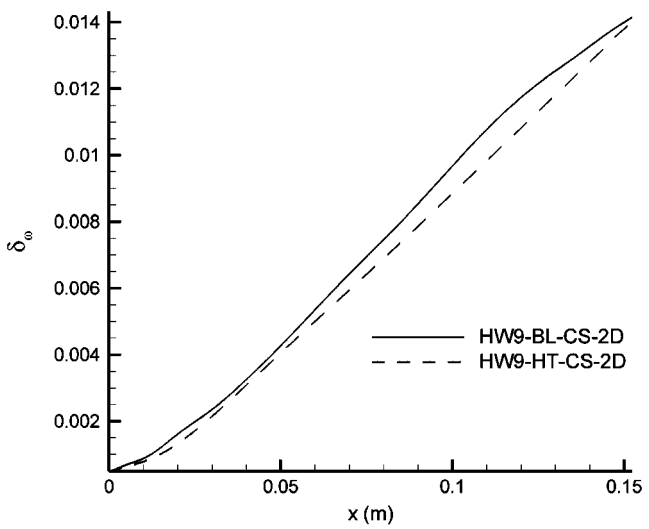

Figure 4. Vorticity thickness variation of two-dimensional HW9 simulations.

Figure 4 shows the vorticity thickness of the two-dimensional mixing layer, using both types of inflow condition. The growth of the layer is largely the same for both inflow conditions, and in Figure 5 the growth rate of the layer can be seen to increase with λ, in agreement with other numerical and experimental results [5, 27]. Similar vorticity thickness variations are found for the BL inflow simulations. These growth rates are not compared with the reference experiment data, as the streamwise extent of the computational domain is insufficient to satisfy the $1000\theta_{\mathrm{m}}$ criterion

DOI: 10.1002/fld

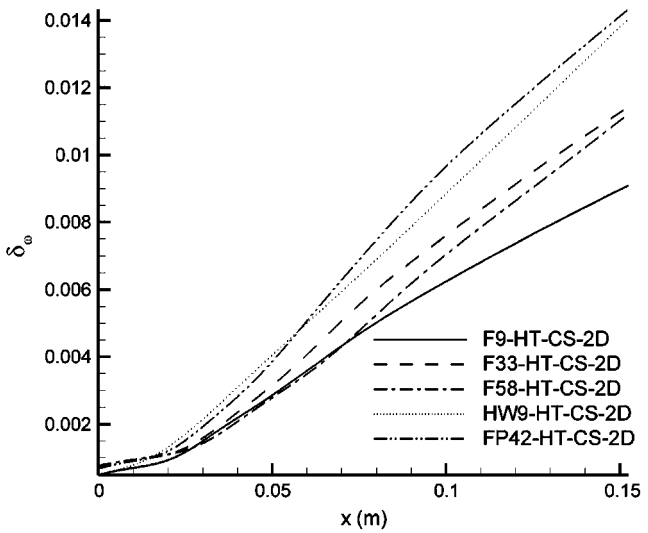

Figure 5. Vorticity thickness variation of the two-dimensional boundary layer inflow condition simulations.

for the flow to attain self-similarity, where θ_{m} is the momentum thickness of the high-speed side boundary layer. In addition, measurements of the thickness of the layer in the experiment began downstream of the streamwise extent of the current computational domain. On the basis of these mean flow statistics, it is straightforward to understand how some researchers have suggested that a two-dimensional simulation of a mixing layer using a hyperbolic tangent inflow condition is sufficient to produce quantitative comparisons to experiment [14, 26, 27].

Figure 6 shows a typical instantaneous output from the two-dimensional simulations. Initially, it appears that both simulations are very similar in appearance, with the initial K–H roll-up forming, and the layer growing through successive pairings caused by the growth of the subharmonics of the fundamental instability. Closer inspection, however, reveals a subtle difference between the two simulations—in the BL inflow case the primary K–H rollers show a large excess of fluid that has originated from the high-speed side. The vortices present in the hyperbolic tangent inflow simulation do not have this excess in the primary rollers, and it appears that the fluid contained within these cores lies in the mid-range of values allowed in the scalar field. Qualitatively, this shows a marked difference in the initial evolution of the layer between the inflow types.

In order to quantify this apparent difference in the make-up of the vortices present in the layer, an expression can be defined to obtain the mean volume fraction of high-speed side fluid contained within the mixing layer. This is given by

$$V_{\mathrm{h}} = \frac{1}{|\delta_{\mathrm{h}} - \delta_{\mathrm{l}}|} \int_{\delta_{\mathrm{l}}}^{\delta_{\mathrm{h}}} \overline{T(\eta)}\, \mathrm{d}\eta \tag{16}$$

where η is the normalized self-similar co-ordinate system, and δ_{h} and δ_{l} are the mean 'boundaries' of the mixing layer, where the scalar T has a value of 0.99 and 0.01, respectively. A similar expression can be obtained for the volume fraction of fluid, V_{l}, that originated from the low-speed side stream. These values can be used to calculate the composition ratio of the layer, which is

DOI: 10.1002/fld

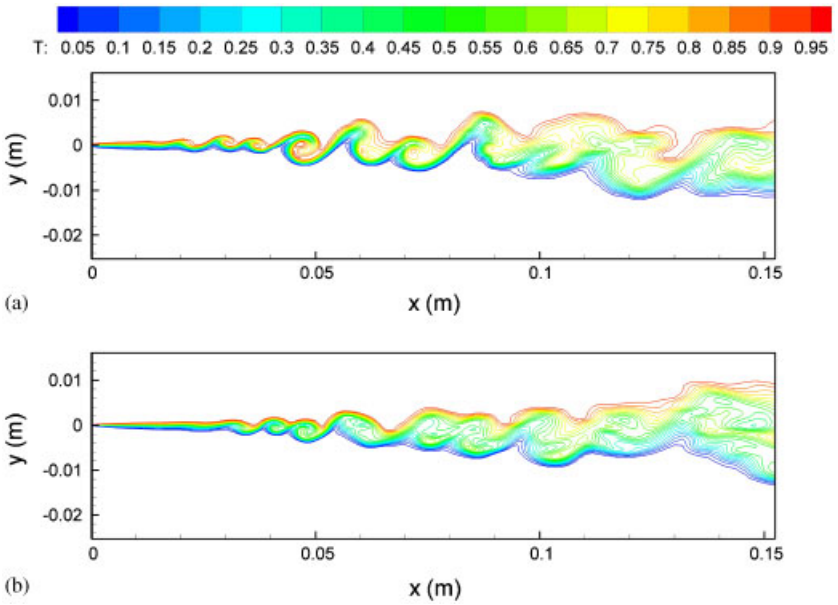

Figure 6. Typical spanwise-averaged scalar fields in cases: (a) F33-HT-CS-2D and (b) F33-BL-CS-2D.

Table II. Composition ratio values of the two-dimensional simulations at $x = 0.13$ m.

Simulation	λ	E_v
F9-HT-CS-2D	0.42	1.27
F9-BL-CS-2D	0.42	1.55
F33-HT-CS-2D	0.49	1.43
F33-BL-CS-2D	0.49	1.58
F58-HT-CS-2D	0.49	1.25
F58-BL-CS-2D	0.49	1.68
HW9-HT-CS-2D	0.54	1.36
HW9-BL-CS-2D	0.54	1.64
FP42-HT-CS-2D	0.61	1.52
FP42-BL-CS-2D	0.61	1.69

defined as

$$E_v = \frac{V_\mathrm{h}}{V_\mathrm{l}} \tag{17}$$

Table II shows the composition ratios for each of the two-dimensional simulations conducted at $x = 0.13$ m. The data show that the composition ratio of the BL inflow simulations is significantly higher than for the counterpart hyperbolic tangent simulations, confirming the qualitative observation above. Both types of simulation to show a composition ratio of greater than one, implying that the layer entrains more fluid from the high-speed side.

DOI: 10.1002/fld

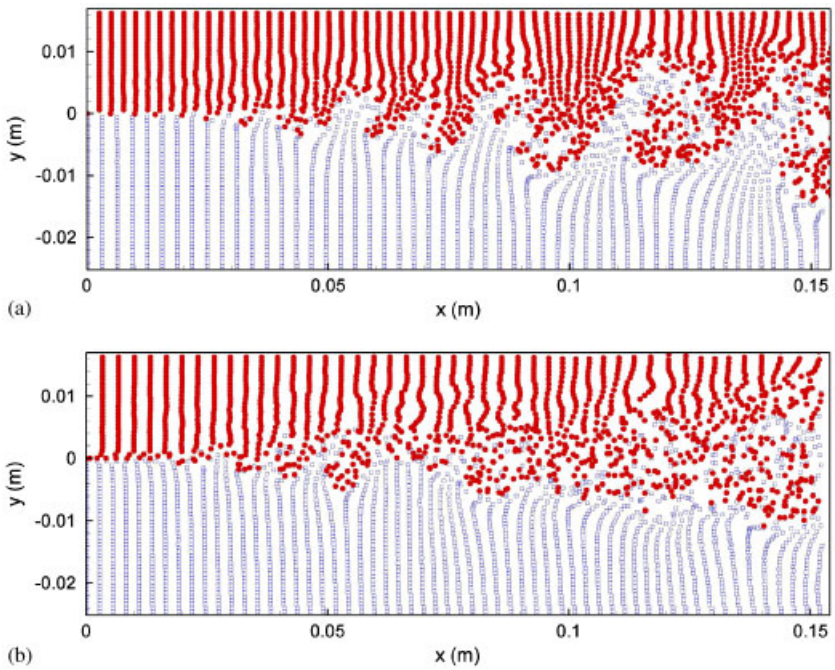

Figure 7. Particle distributions for: (a) F9-HT-CS-2D and (b) F9-BL-CS-2D.

In order to study the effect that the inflow condition has on the initial evolution of the mixing layer, massless tracer particles are injected into the flow at the inflow plane. The particles are injected into the layer in such a way that their number density is equal in both free streams. As the particles are massless, their motion is governed by the equation

$$\mathbf{x}_\mathrm{p} = \int_t^{t+\Delta t} \mathbf{U}_\mathrm{p}\, \mathrm{d}t \tag{18}$$

Figure 7 shows a typical instantaneous particle distribution field for the two-dimensional simulations. Again, they are qualitatively similar, with the familiar 'swiss-roll' pattern indicating that fluid is entrained into the layer by the pairing process. However, a close-up of the first few centimetres of this image in Figure 8 illustrates that the initial behaviour of the layer is markedly different in each simulation. In the hyperbolic tangent case, all the particles near the centreline of the layer convect downstream with a velocity of approximately that of the mean convection velocity U_a. The streamwise velocity at the inflow plane in the BL inflow simulations, however, is near-zero due to the no-slip boundary conditions applied in the precursor boundary layer simulations. This means that there is a small, wake-like region just downstream of the inflow plane, where the two streams merge and form the inflectional velocity profile required for the layer to roll up into K–H vortices. For such an inflow condition, the instability develops before the boundary layers have fully merged, and subsequently a parallel shear layer is not established. It is known that the high-speed boundary layer contains most of the vorticity initially present within the real flow [40], as the vorticity in

DOI: 10.1002/fld

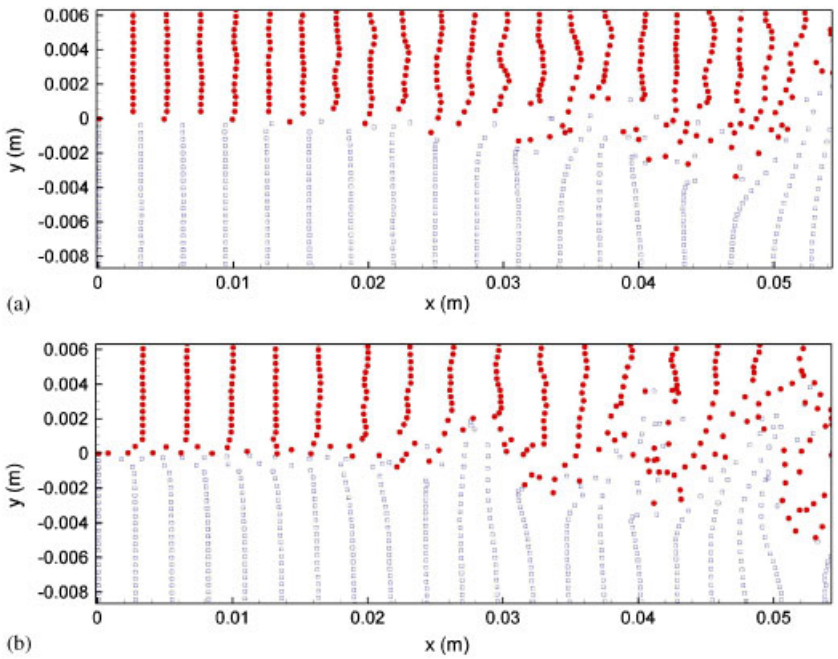

Figure 8. Close-up view of particle distributions in the wake region for: (a) F9-HT-CS-2D and (b) F9-BL-CS-2D.

the low-speed boundary layer is rapidly cancelled by the vorticity of the opposite hand from the high-speed side fluid. This results in the inflection point in the velocity profile being established in the high-speed side of the fluid, giving the large excess of fluid found in the primary K–H roll-up.

Inspection of Equation (11) reveals that the hyperbolic tangent profile used in these simulations is symmetric in nature, and as such the initial circulation that it provides, will be focused on the centreline of the layer, and as a consequence, at the scalar interface between the two streams. This will result in fluid being drawn roughly equally from both streams into the initial K–H roll-up, and therefore produce the large discrepancy in the composition of the primary vortex formed in the layer, when compared to the BL inflow simulations.

It should be noted that the merging of the boundary layers only influences the composition of the fluid within the initial roll-up and does not affect the entrainment of fluid during pairing interactions as the flow progresses downstream. For example, the composition ratio at $x = 0.03$ m in case F33-BL-CS-2D is 3.55, whilst case F33-HT-CS-2D has a value of 1.11 at the same location. Comparison with the values recorded at $x = 0.13$ m in Table II reveals that the discrepancy is not as large, highlighting two issues. Firstly, as the flow develops, the fluid entrained during the roll-up process in the BL inflow simulations is diluted as pairing interactions entrain fluid from the free streams. Secondly, the entrainment of fluid from the free streams is biased towards the high-speed fluid, and given a sufficiently long computational domain, the composition ratio of the layer produced by both inflow conditions will relax to the value of the entrainment ratio between the free streams.

DOI: 10.1002/fld

Clearly, this discrepancy in the composition ratio of the layer has wide-ranging effects on the numerical simulation of the mixing layer flow, particularly in terms of chemically reacting and combusting shear layers, where the reaction rate and combustion sustainability is determined by the composition of the fluid within the structures.

4.2. Three-dimensional simulations

The above simulations are repeated with the addition of the spanwise domain, which permits the extra degree of freedom that is found in the real flow. Typical mean and RMS flow quantities are presented in Figures 2 and 3, along with the data from its two-dimensional counterpart simulation. The mean streamwise velocity profile again agrees well with the experimental data, and the RMS streamwise velocity fluctuations produce a much better comparison to experiment. The cross-stream fluctuations have a peak magnitude that is significantly lower than the counterpart two-dimensional simulations, and this is due to the presence of the spanwise dimension, and the subsequent transfer of energy into the turbulent fluctuations in this flow direction. The kink in the mean scalar profile is much less pronounced in the three-dimensional simulations, and it, along with the bimodal profile of the RMS of the scalar fluctuation, disappears with downstream distance in the three-dimensional simulations, as shown in Figure 3. The change in the scalar profiles is due to the transition to turbulence in the mixing layer flow. The transition is triggered by the three-dimensional interaction between the primary vortices and the secondary streamwise structures during a pairing of the former, and its mean transition location has been considered in detail elsewhere [37, 41]. The vorticity thickness variations of cases F9-BL-CS-3D, HW9-BL-CS-3D, and their counterpart two-dimensional simulations are shown in Figure 9, with the three-dimensional flows growing much more quickly than when the flow is confined to two dimensions.

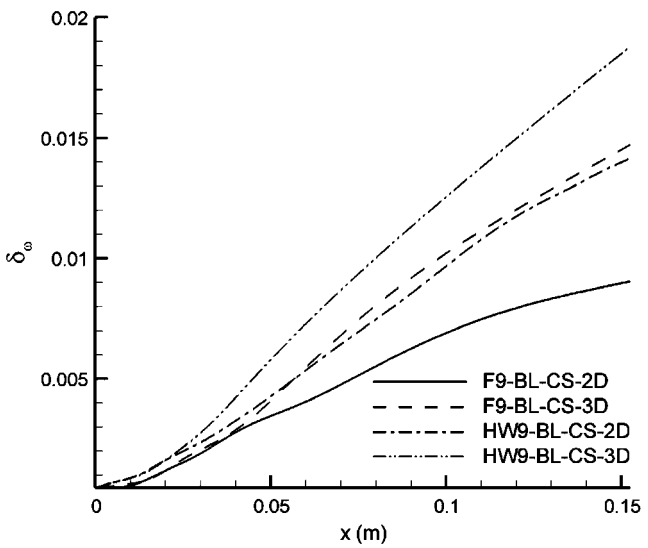

Figure 9. Vorticity thickness of F9-BL-CS-3D, HW9-BL-CS-3D, and their two-dimensional counterpart simulations.

DOI: 10.1002/fld

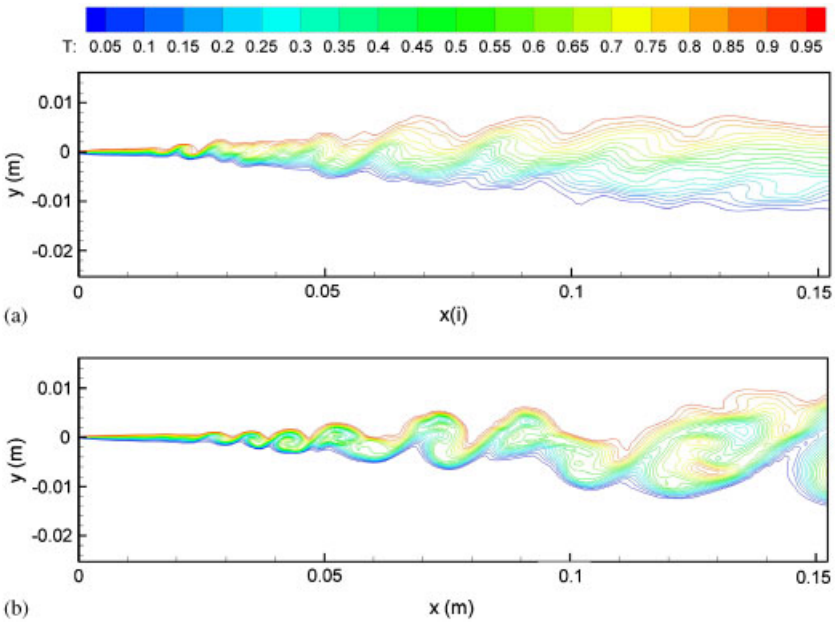

Figure 10. Comparison of spanwise-averaged scalar fields between: (a) F33-HT-CS-2D and (b) F33-HT-CS-3D.

The scalar images taken from the three-dimensional simulations are spanwise-averaged, in order to give a reasonable, yet not direct comparison to the schlieren and shadowgraph images found in some experimental work [5, 30, 42]. Such a flow field is presented in Figure 10 from case F33-HT-CS-3D along with a similar image from case F33-HT-CS-2D. The most striking difference between the two fields is that the structures in the three-dimensional simulation appear markedly different in form to those in the two-dimensional system, downstream of $x = 0.07$ m. The reasons for this visual difference are twofold; firstly, the spanwise-averaging procedure tends to 'smooth out' the variations in the scalar within the structures, resulting in the relatively uniform scalar distribution present within the large-scale structures. Secondly, the flow in the three-dimensional simulation has undergone a transition to turbulence, resulting in a change in the distribution of vorticity within the structure. In the pre-transition flow, as in the two-dimensional simulations, the vorticity in each of the large vortices remains concentrated in a relatively compact core, whilst post-transition, the vorticity is much more evenly distributed throughout the coherent vortex. This change in the vorticity distribution implies that the post-transition structures contain fluid that is much more uniformly mixed. The presence of secondary streamwise vortices is required for the layer to undergo transition to turbulence [43], and as the two-dimensional simulations are incapable of capturing this phenomena, the flow in such runs does not undergo a transition to turbulence, instead remaining in an unsteady yet laminar state.

The composition ratio at $x = 0.13$ m in each of the simulations is shown in Table III, along with the mean transition location of the flow, x_t. This transition location was calculated by two means—firstly, frequency spectra were recorded at several streamwise locations, and the position where the roll-off in the spectra approached $-\frac{5}{3}$ was noted. Secondly, sequences of flow outputs, such as

DOI: 10.1002/fld

Table III. Composition ratio values of the three-dimensional simulations at $x = 0.13$ m, with the mean transition location of the flow.

Simulation	λ	E_v	x_t
F9-HT-CS-3D	0.42	0.97	0.065
F9-BL-CS-3D	0.42	1.27	0.068
F33-HT-CS-3D	0.49	1.03	0.07
F33-BL-CS-3D	0.49	1.35	0.071
F58-HT-CS-3D	0.49	1.03	0.082
F58-BL-CS-3D	0.49	1.33	0.085
HW9-HT-CS-3D	0.54	0.98	0.062
HW9-BL-CS-3D	0.54	1.26	0.065
FP42-HT-CS-3D	0.61	0.99	0.076
FP42-BL-CS-3D	0.61	1.34	0.08

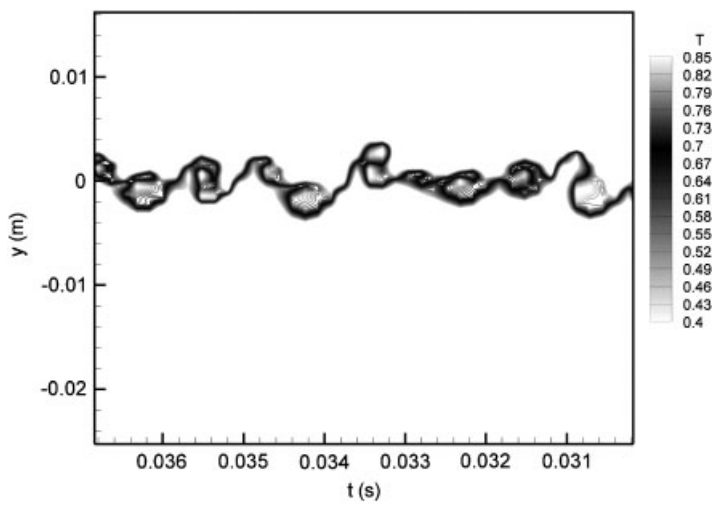

Figure 11. Time trace through $x = 0.05$ m in case F58-BL-CS-2D.

vorticity and scalar fields were recorded at intervals of $100\Delta t$, and the positions of the interactions that precipitated the transition to turbulence were recorded. These data were then combined to arrive at the values in Table III. Surprisingly, a three-dimensional simulation using a hyperbolic tangent inflow condition produces a post-transition composition ratio that is approximately equal to one. This infers that the mixing layer entrains equal amounts of fluid that originated from both free streams, in complete contradiction to the experimental work of Konrad [6] and Koochesfahani and Dimotakis [7]. The BL inflow case, however, produces a composition ratio that compares much more favourably with the data from those two experiments. Interestingly, the composition ratios of the two-dimensional simulations initialized from a hyperbolic tangent function are very close to those found in three-dimensional simulations initiated by a BL inflow condition. This close relationship is entirely coincidental, as the unrealistically low initial entrainment in the former case is offset by more rapid flow development upstream of the sampling station. This flow development continues throughout the flow and results in higher compositions found downstream of the sampling station.

DOI: 10.1002/fld

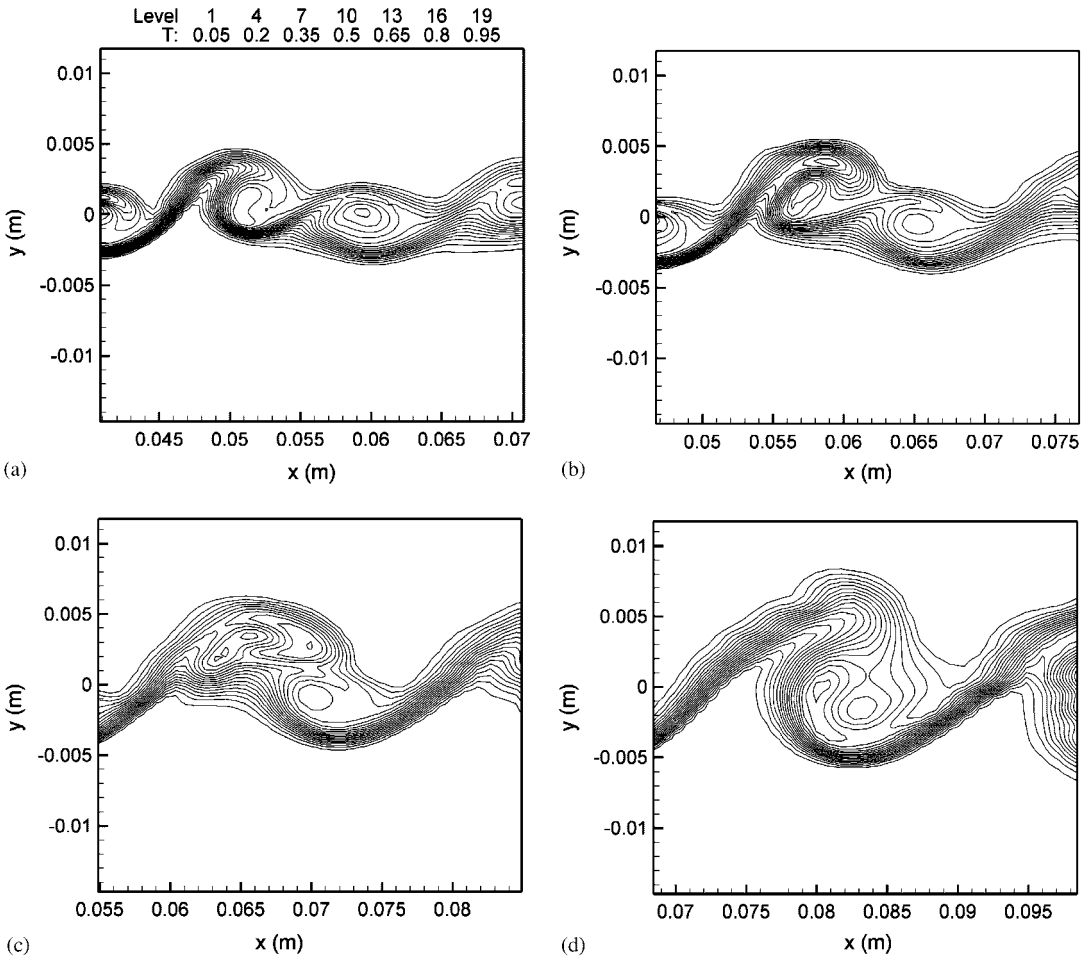

Figure 12. Typical pairing interaction of vortices in the two-dimensional simulations.

The three-dimensional simulations with BL inflow do not show this behaviour, with the composition ratio of simulations of this type remaining roughly constant downstream of the sampling station.

4.3. Mechanisms of growth

The majority of past research into the mixing layer flow has shown that the growth of the layer is dominated by the interactions between the primary spanwise vortices present in the flow. The interactions that occur between both the pre-transition vortices, and the coherent structures in the turbulent region of the flow are widely believed to take the form of vortex pairing found in experimental [44] and numerical research [14, 29, 45]. In Figures 10(a) and (b), it is obvious that the number density of the vortices in the flow decreases with downstream distance from the inflow plane, suggesting that interactions are taking place to achieve this. The presence of large vortices beyond the transition location in Figure 10(a) (beyond $x = 0.07$ m in this case) is indicated by

DOI: 10.1002/fld

the clustering of the scalar lines in the braid region between the structures, and the 'bumps' on the edges of the layer where these braids wrap themselves around the cores of the structures. Sequences of scalar images stored from the simulations at intervals of $100\Delta t$ are analysed to elucidate the types of interactions that take place between the structures. Time traces—where the flow passing through a streamwise control plane is recorded over a long time period—are also used to aid in this process. This time trace method is a two-dimensional analogy of the work of Jimenez *et al.* [46].

4.3.1. Two-dimensional simulations. A time trace of the flow passing through $x = 0.05$ m of case F58-BL-CS-2D is shown in Figure 11. The time axis of the time trace images is reversed so that the structures have the same orientation as the instantaneous spatial images. The vortices in the flow passing through this control plane are quite clearly displacing laterally within the layer, in order to undergo a process of amalgamation-by-pairing. A typical interaction of this type is shown in Figure 12. In Figure 12(a), the two vortices are shown to be in roughly the same lateral location in the layer. In Figures 12(b) and (c), the upstream vortex rotates over the top of the downstream structure, and the lateral displacement of the vortices entrains fluid from the free streams. In Figure 12(d), the amalgamation of the vortices is complete, and produces the increase in the visual thickness of the layer. Pairing interactions of this type are brought about due to growth of a subharmonic of the fundamental instability, and the interaction process seen in the simulations is entirely consistent with those noted elsewhere [44]. Amalgamative pairings of this form are evident throughout the computational domain of the two-dimensional simulations, regardless of the type of inflow condition used to initiate the layer, and the principal mechanism of growth in the two-dimensional mixing layer simulation is through these pairing interactions.

4.3.2. Three-dimensional simulations. A typical time trace of the flow in the pre-transition region of the three-dimensional mixing layer simulations is shown in Figure 13, recorded at $x = 0.05$ m

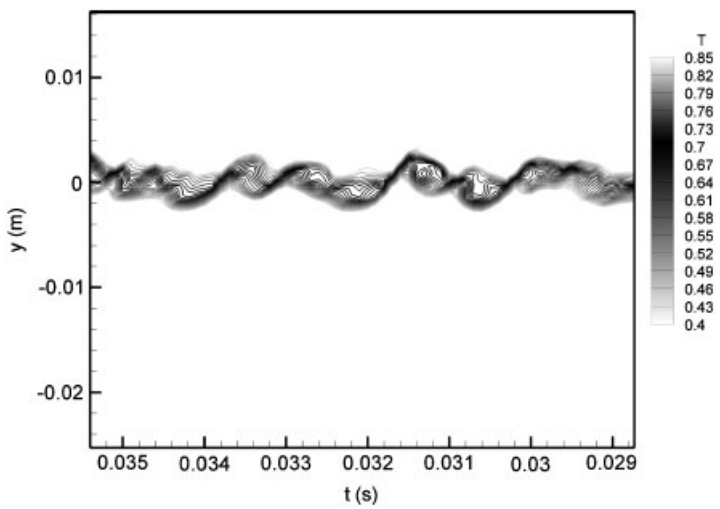

Figure 13. Time trace through $x = 0.05$ m in case FP42-BL-CS-3D.

DOI: 10.1002/fld

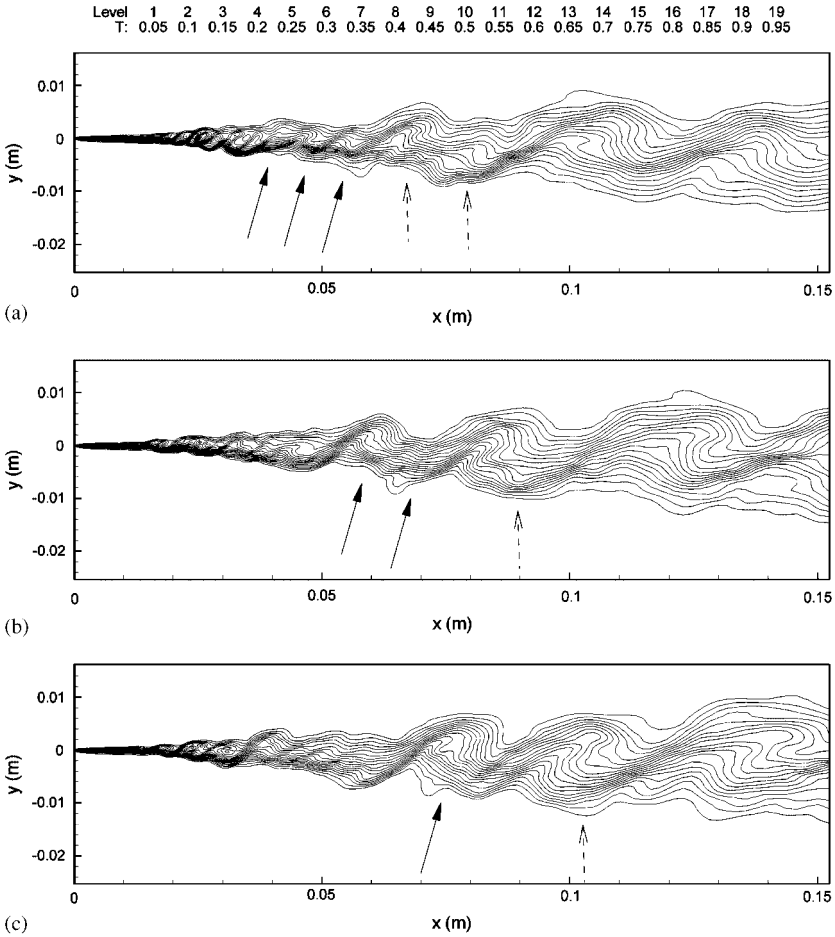

Figure 14. Sequence of images demonstrating the interactions that occur between pre-transition vortices in the three-dimensional mixing layer.

from case FP42-BL-CS-3D. The procedure of spanwise-averaging the passive scalar removes much the definition of the individual vortices, although evidence of lateral displacement of vortices within the layer is apparent. The nature of the interactions between vortices in this region of the flow is very similar to that found in the two-dimensional flow (Figure 12), with the vortices rotating around each other and amalgamating, causing an increase in the visual thickness of the layer. The interactions that occur between the vortices can also involve three separate structures—a process that is known as a *tripling* interaction. Figure 14 shows a sequence of images capturing such an event. In Figure 14(a), the structures marked with dashed arrows are undergoing a normal amalgamation-by-pairing event, similar to that presented in Figure 12. The three upstream vortices, marked with the solid arrows, also begin to interact in a similar manner. In Figure 14(b), the three vortices are amalgamating to form a new structure, with the two furthest upstream of the three vortices rotating over its downstream neighbour. The interaction is completed in image (c), with a

DOI: 10.1002/fld

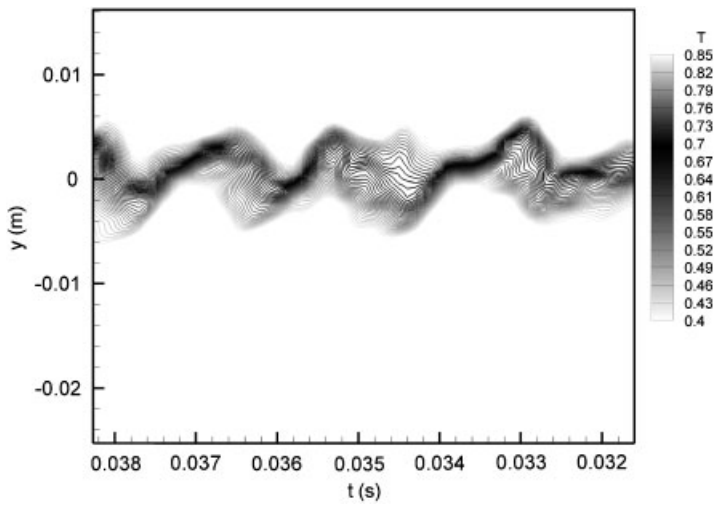

Figure 15. Time trace through $x = 0.13$ m in case F9-BL-CS-3D.

new large-scale turbulent structure formed. Analysis of sequences of the spanwise-averaged scalar field suggests that there is no hierarchical ordering to these interactions. Both the pairing and tripling interactions highlighted in Figure 14 trigger the transition to turbulence within the flow, in agreement with other experimental and numerical research [43, 45].

Beyond the mixing transition, the process by which the coherent structures interact is not quite so clear. A time trace was recorded at a streamwise location of $x = 0.13$ m from cases F9-BL-CS-3D and is shown in Figure 15. The structures, separated by braid regions where the scalar filed lines are angled at 45 degrees to the flow, do not appear to rotate around each other in order to undergo amalgamation-by-pairing-type interactions. Similar time traces are obtained in the post-transition region of all the three-dimensional simulations conducted here, and no pairing interactions that are symptomatic of the type shown in Figure 12 are obvious beyond the mixing transition. The data presented here suggest that not only does the mixing transition in the mixing layer bring about a change in the pattern and extent of molecular-scale mixing in the flow [6, 7], but it also brings about a change in the growth mechanism of the layer. The large-scale structure marked with the dashed arrow in (b) and (c) of Figure 14 and its downstream neighbour demonstrate this as these structures appear to remain in a fixed lateral position as they travel downstream, growing in size in a continuous manner. This type of continuous growth has been noted previously by Hernan and Jimenez [47], who determined that much of the growth of the layer was associated with the continuous growth of the individual structures. The present simulations are consistent with this experimental evidence and, more particularly, with the results of more recent experiments which have indicated that the pairing-driven and continuous growth mechanisms are characteristic of the pre- and post-transition flows, respectively [30, 48].

5. CONCLUSIONS

Simulations of spatially developing mixing layers have been conducted, using two separate inflow conditions, and in both two and three dimensions. The effects of the inflow condition on the layer

DOI: 10.1002/fld

are analysed, along with the mechanisms of growth that govern both the two- and three-dimensional mixing layers.

A large difference between the composition of two-dimensional mixing layers that are initialized by either a hyperbolic tangent function or precursor boundary layer inflow data has been noted. Mixing layers produced by a boundary layer inflow condition have composition ratios that are much higher than those found in layers initialized by a hyperbolic tangent function, and this is due to the positioning of the circulation present in the layer with respect to the interface of the scalar within the flow. Both sets of two-dimensional simulations entrain fluid preferentially from the high-speed side stream of the flow.

The contrast in the properties of two- and three-dimensional mixing layers is assessed. In the two-dimensional simulations a transition to turbulence is not captured, leading to the comparatively poor self-similar flow characteristics reported here, when compared with counterpart three-dimensional runs. As a result, the two-dimensional simulations should be considered to be in an unsteady laminar state. The transition to turbulence is captured in the three-dimensional simulation, and large-scale coherent structures are found in the post-transition region of the flow. The structures are composed of fluid that is much more thoroughly mixed than at the same streamwise locations in the two-dimensional simulations. The composition ratio of the three-dimensional layers is much different to their two-dimensional counterparts, with the hyperbolic tangent inflow cases yielding a composition ratio of unity, contradicting previous experimental evidence. Three-dimensional simulations conducted with boundary layer inflow data produce composition ratios that agree favourably with experiment, as more fluid is entrained from the high-speed side fluid.

The above points demonstrate that two-dimensional simulations are wholly insufficient to provide an accurate description of the real mixing layer flow. This and the unrealistic composition ratio of the three-dimensional mixing layer initialized from a hyperbolic tangent function have significant impact on the modelling of chemically reacting and combusting flows, and indicate that in order to successfully replicate the behaviour of the real flow, the initial conditions of the flow must be matched *as closely as possible* to that of the experiment, otherwise inaccurate results will be obtained.

The mechanisms that drive the growth of the mixing layer are studied. The well-known growth by amalgamative pairings of vortices drives the growth of the two-dimensional simulations and also dominates the pre-transition region of the three-dimensional mixing layer flow. Beyond the mixing transition the dominant mechanism of growth is not so obvious. Pairing interactions are not observed, and the coherent structures embedded in the flow appear to grow in a continuous manner. The mechanism of growth in the flow beyond the mixing transition is not determined, as the streamwise extent of the computational domain is insufficient to gather detailed information on this region of the flow. Details of this continuous growth beyond the mixing transition are beyond the scope of this article, and will be examined elsewhere [49, 50].

REFERENCES

1. Liepmann HW, Laufer J. Investigation of free turbulence mixing. *NACA Technical Note No. 127*, 1947; **36**(5): 765–781.
2. Wygnanski I, Fielder HE. The two-dimensional mixing region. *Journal of Fluid Mechanics* 1970; **41**:317–361.
3. Batt RG. Some measurements on the effect of tripping the two-dimensional shear layer. *AIAA Journal* 1975; **13**:245–247.
4. Rodi W. *Review of Experimental Data of Uniform Density Free Turbulent Boundary Layers*. University of Karlsruhe: Germany, 1975.

DOI: 10.1002/fld

5. Brown GL, Roshko A. On density effects and large structure in turbulent mixing layers. *Journal of Fluid Mechanics* 1974; **64**:755–816.
6. Konrad JH. An experimental investigation of mixing in two-dimensional shear flows with applications to diffusion limited chemical reactions. *Ph.D. Thesis*, California Institute of Technology, California, 1976.
7. Koochesfahani MM, Dimotakis PE. Mixing and chemical reactions in a turbulent liquid mixing layer. *Journal of Fluid Mechanics* 1986; **170**:83–112.
8. Riley JJ, Metcalfe RW, Orszag SA. Direct numerical simulations of chemically reacting turbulent mixing layers. *Physics of Fluids* 1986; **29**:406–421.
9. Rogers MM, Moser RD. The three-dimensional evolution of a plane mixing layer: the Kelvin–Helmholtz rollup. *Journal of Fluid Mechanics* 1992; **243**:183–226.
10. Metcalfe RW, Orszag SA, Brachet ME, Menon S, Riley JJ. Secondary instability of a temporally growing mixing layer. *Journal of Fluid Mechanics* 1987; **187**:207–243.
11. Moser RD, Rogers MM. The three-dimensional evolution of a plane mixing layer: pairing and transition to turbulence. *Journal of Fluid Mechanics* 1993; **247**:275–320.
12. Moser RD, Rogers MM. Mixing transition and the cascade to small scales in a plane mixing layer. *Physics of Fluids A* 1991; **3**:1128–1134.
13. Lebœuf RL, Metha RD. Core instability of the spanwise vortices in a plane mixing layer. *Physics of Fluids A* 1995; **7**:1516–1518.
14. Yang WB, Zhang HQ, Chan CK, Lin WY. Large eddy simulation of mixing layer. *Journal of Computational and Applied Mathematics* 2004; **163**:311–318.
15. Wang JK, Milane RE. Large eddy simulation (2D) of spatially developing mixing layer using vortex-on-cell for flow field and filtered probability density function for scalar field. *International Journal for Numerical Methods in Fluids* 2006; **50**:27–61.
16. Tenaud C, Pellerin S, Dulieu A, Ta Phouc L. Large eddy simulations of a spatially developing incompressible 3D mixing layer using the v–ω formulation. *Computational Fluids* 2005; **34**:67–96.
17. de Bruin ICC. Direct and large eddy simulation of the spatial turbulent mixing layer. *Ph.D. Thesis*, University of Twente, Twente, 2001.
18. Comte P, Silvestrini JH, Bégou P. Streamwise vortices in large eddy simulations of mixing layers. *European Journal of Mechanics B/Fluids* 1998; **4**:615–637.
19. Vreman B, Geurts B, Kuerten H. Self-similar states in turbulent mixing layers. *Journal of Fluid Mechanics* 2001; **446**:1–24.
20. Li N, Balaras E, Piomelli U. Inflow conditions for large eddy simulation of mixing layers. *Physics of Fluids* 2000; **12**:935–938.
21. Zhou XY, Pereira JCF. Large eddy simulation (2D) of a reacting plane mixing layer using filtered density function closure. *Flow Turbulence and Combustion* 2000; **64**:279–300.
22. Oster D, Wygnanski I. The forced mixing layer between parallel streams. *Journal of Fluid Mechanics* 1982; **123**:91–130.
23. Balaras E, Piomelli U, Wallace JM. Self-similar states in turbulent mixing layers. *Journal of Fluid Mechanics* 2001; **446**:1–24.
24. Whitfield D, Swafford T, Jacocks J. Calculation of turbulent boundary layers with separation, reattachment and viscous–inviscid interaction. *AIAA-80-1439*, 1980.
25. Lésieur M, Staquet C, Le Roy P, Comte P. The mixing layer and its coherence examined from the point of view of two-dimensional turbulence. *Journal of Fluid Mechanics* 1988; **192**:511–534.
26. Jaberi FA, Colucci PJ, James S, Givi P, Pope SB. Filtered mass density function for large-eddy simulation of turbulent reacting flows. *Journal of Fluids Mechanics* 1999; **401**:82–121.
27. Yang WB, Zhang HQ, Chan CK, Lau KS, Lin WY. Investigation of plane mixing layer using large eddy simulation. *Computational Mechanics* 2004; **34**:423–429.
28. Givi P. Model free simulations of turbulent reactive flows. *Progress in Energy Combustion Sciences* 1989; **15**:1–107.
29. Ghoniem AF, Ng K. Numerical study of the dynamics of a forced shear layer. *Physics of Fluids* 1987; **30**:706–721.
30. D'Ovidio A. Coherent structures in turbulent mixing layers. *Ph.D. Thesis*, University of Leicester, Leicester, 1998.
31. Roache PJ. *Computational Fluid Dynamics*. Hermosa Publishers: Albuquerque, New Mexico, 1972.
32. Gao S, Voke PR. Large eddy simulations of turbulent heat transport in enclosed impinging jets. *International Journal of Heat and Fluid Flow* 1993; **16**5:377–393.
33. Smagorinsky J. General circulation experiments with the primitive equations. *Monthly Weather Review* 1963; **91**:99–164.

DOI: 10.1002/fld

34. Germano M, Piomelli U, Moin P, Cabot W. A dynamic subgrid-scale eddy viscosity model. *Physics of Fluids A* 1991; **3**:1760–1765.
35. Lilly DK. A proposed modification of the Germano subgrid-scale closure method. *Physics of Fluids A* 1992; **4**:633–635.
36. Métais O, Lesieur M. Spectral large eddy simulations of isotropic and stably-stratified turbulence. *Journal of Fluid Mechanics* 1992; **239**:157–194.
37. McMullan WA, Gao S, Coats CM. Large eddy simulation of transition to turbulence in spatially developing mixing layers. Under Review.
38. Courant R, Friedrichs KO, Lewy H. Über die partiellen differentialgleichungen der mathematischen Physik. *Mathematische Annalen* 1928; **100**:32–74.
39. Inoue O. Vortex simulation of a turbulent mixing layer. *AIAA Journal* 1985; **23**:367–373.
40. Monkewitz PA, Heurre P. Influence of the velocity ratio on the spatial instability of mixing layers. *Physics of Fluids* 1982; **27**:1137–1143.
41. McMullan WA, Gao S, Coats CM. Large eddy simulation of transition to turbulence in spatially developing mixing layers using a realistic inflow condition. Under Review.
42. Bernal LP, Roshko A. Streamwise vortex structures in plane mixing layers. *Journal of Fluid Mechanics* 1986; **170**:499–525.
43. Huang L, Ho CM. Small scale transition in a plane mixing layer. *Journal of Fluid Mechanics* 1990; **210**:475–500.
44. Winant CD, Browand FK. Vortex pairing: the mechanism of turbulent mixing layer growth at moderate Reynolds numbers. *Journal of Fluid Mechanics* 1974; **63**:237–255.
45. Moser RD, Rogers MM. The three-dimensional evolution of a plane mixing layer: pairing and transition to turbulence. *Journal of Fluid Mechanics* 1993; **247**:275–320.
46. Jimenez J, Cogollos M, Bernal LP. A perspective view of the plane mixing layer. *Journal of Fluid Mechanics* 1985; **152**:125–143.
47. Hernan MA, Jimenez J. Computer analysis of a high-speed film of a plane turbulent mixing layer. *Journal of Fluid Mechanics* 1982; **119**:323–345.
48. Coats CM. Coherent structures in combustion. *Progress in Energy Combustion Sciences* 1996; **22**:427–509.
49. D'Ovidio A, Coats CM. Coherent-structure evolution in turbulent mixing layers. Part 1: Experimental evidence. Under Review.
50. McMullan WA, Gao S, Coats CM. Coherent-structure evolution in turbulent mixing layers. Part 2: Large eddy simulation. Under Review.

DOI: 10.1002/fld